Nuclear Inst. and Methods in Physics Research, A 1052 (2023) 168288

Contents lists available at ScienceDirect

Nuclear Inst. and Methods in Physics Research, A

journal homepage: www.elsevier.com/locate/nima

Full Length Article

Transformation of ICEBall to fIREBall for conversion electron spectroscopy

Kevin Lee [a,*], Christina Dulal [a], Wanpeng Tan [a], Armen Gyurjinyan [b], Ethan Sauer [a], Shelly Lesher [c], Ani Aprahamian [a]

[a] Department of Physics and Astronomy, University of Notre Dame, Notre Dame, IN, 46556, USA
[b] A. Alikhanyan National Science Laboratory of Armenia, Yerevan, Armenia
[c] Department of Physics, University of Wisconsin–La Crosse, La Crosse, WI 54601, USA

ARTICLE INFO

Keywords:
Conversion electron spectroscopy
Nuclear structure
Mini-orange electron spectrometer
ICEBall
fIREBall
Electron-gamma coincidences
E0 transitions
Conversion coefficients

ABSTRACT

Conversion electron spectroscopy is a valuable tool in nuclear structure studies, but the complex spectra resulting from the high density of levels in the spectra of heavy nuclei make it difficult to extract the most beneficial information from singles measurements. This work reports on the transformation of ICEBall, which was a mini-orange spectrometer that was used in coincidence with various Germanium detector arrays, to the improved fInternal conveRsion Electron Ball (fIREBall) spectrometer for the improved measurements of E0 transitions and conversion electron coefficients. A combination of FreeCAD, COMSOL, and Geant4 simulations were implemented to optimize the geometries for the magnet filters used in the spectrometer to significantly improve the efficiency of electron collection in the energy range of interest 200 keV-1 MeV. The array of six mini-orange Si(Li) detectors are to be replaced with six new, thicker Si(Li) detectors. Experimental tests reported here show a peak improvement in absolute efficiency from 2.8% to 5.3% for the 482 keV K electron line in ^{207}Bi for a single magnet filter and detector pair.

1. Introduction

Conversion electron spectroscopy and the measurements of E0 transitions are valuable tools for nuclear structure. Conversion electron and gamma spectroscopy in-coincidence measurements can be used to clearly identify specific transitions and their conversion coefficients [1]. Enhanced E0 transitions between 0^+ states have long been recognized as definitive proof for co-existence of different shapes. The open question in nuclear structure regarding the existence and onset of collectivity for the low lying $K = 0^+$ excitations continues in spite of abundance reaction rates and lifetime measurements. A review by Heyde and Wood [2] pointed to the measurements of E0 transitions as the additional potentially convincing evidence for distinguishing between the interpretation of low-lying $K = 0^+$ states as collective excitations or the minima of coexisting shapes in the spectra of well deformed nuclei.

The development of techniques for conversion electron spectroscopy in singles have excelled with high precision conversion electron measurements such as the BILL spectrometer [3] at Institut Laue-Langevin in France. The singles electron measurements, however precise, result in very complicated analyses. More recent developments have been towards coincidence measurements of electrons and gamma-rays. The potential of utilizing magnetic fields to separate electrons of different energies has been known since the early 1900s [4]. An early design by Rutherford used a parallel pole electromagnet to create a nearly uniform magnetic field to deflect electrons in a semi-circle trajectory [5]. A search for more efficient ways of generating uniform magnetic fields led to the incorporation of solenoid magnets in spectrometers [6–10] called "lens spectrometers". These setups directed electrons in a helical trajectory and used lensing and baffle systems to filter out a specific energy.

An alternative method eventually emerged which was to arrange electromagnets like pieces of an orange to create a magnet filter. The magnet filters in this "orange spectrometer" setup created a toroidal magnetic field to direct the electrons. These designs allowed the source and the detector to be placed outside of the magnetic field [11–13] and showed an improvement in detection efficiency and resolution over the solenoidal designs [14].

However, the potential of these early spectrometers was limited by some drawbacks. The size of the electromagnets required large enclosures, resulting in an overall large physical size, and meant that other detectors could not be placed close to the source/target. The use of iron and copper in the electromagnets also caused gamma rays to be scattered. These drawbacks reduced the quality of gamma spectra that could be obtained, rendering coincidence measurements nearly impossible. Furthermore, these spectrometers were limited to detecting electrons of a single energy. Electron spectra were obtained by changing the magnetic field strength multiple times to sweep over desired

* Corresponding author.
E-mail address: klee16@nd.edu (K. Lee).

https://doi.org/10.1016/j.nima.2023.168288
Received 28 November 2022; Received in revised form 27 March 2023; Accepted 7 April 2023
Available online 8 April 2023

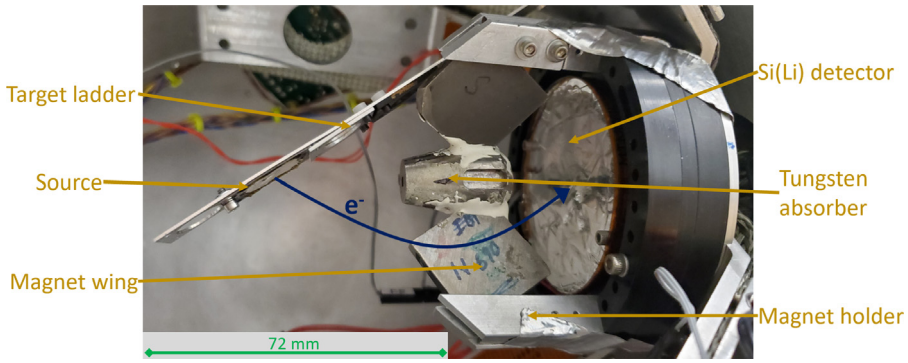

Fig. 1. A single mini-orange magnet filter and Si(Li) pair in ICEBall. The tungsten absorber blocks the direct paths from the source to the detector while the magnet wings create a field of magnetic lines that electrons follow towards the detector. An example trajectory of an electron is drawn in blue. The distance from the target to the detector is 72 mm, indicated by the green scale on the bottom left.

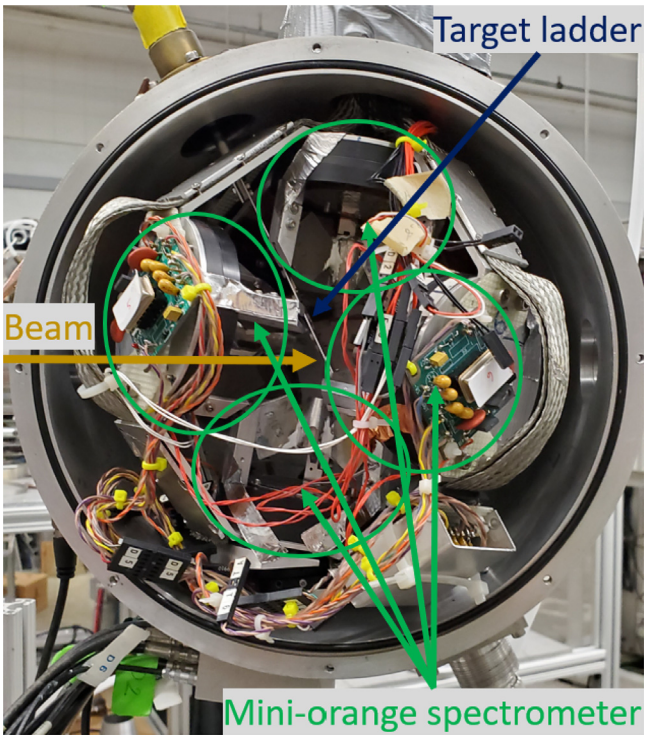

Fig. 2. The interior of the ICEBall array at the Nuclear Science Laboratory at the University of Notre Dame with all six magnet filters and Si(Li) detectors present (labeled in green). Everything is precisely positioned around the target ladder (blue). The beam direction is labeled in gold.

electron energies, which made in-beam experiments time-consuming [14].

New spectrometers were developed to take advantage of the increased availability of semiconducting detectors which allowed simultaneous detection of electrons over a wide energy range with good energy resolution. Solenoidal spectrometers began incorporating superconducting solenoids to create stronger magnetic fields [15–18]. These superconducting solenoids were highly efficient at detecting electrons over a wide energy range, but were also susceptible to high background from gamma rays, delta rays, and heavy particles [14].

The mini-orange spectrometer was pioneered by van Klinken as a successor to the orange spectrometer. Like its predecessor, the mini-orange spectrometer also utilized magnet filters to create a toroidal magnetic field to filter electrons and direct them towards a detector. However, the difference was that the magnetic field was generated by using small permanent magnets mounted on a central absorber [19]. Like the superconducting solenoid, it was able to detect electrons over a wide energy range. While it was less efficient than the superconducting solenoid at detecting electrons, the mini-orange was superior in rejecting the unwanted gamma rays, delta rays, and heavy particles. Its compact size and simple construction also allowed it to be easily integrated in gamma ray detector arrays, making it ideal for coincidence measurements [20].

The ideal configuration of the magnet filters has been an area of exploration within the development of mini-orange spectrometers. The number of wings, the shape of the magnet, and the composition material are all parameters that can affect the magnetic field generated from the wings. This directly affects the detection efficiency of conversions electrons as different magnetic field strengths can be optimal for directing different ranges of electron energies towards the detector [21,22].

Alternative methods have also emerged during the evolution of spectrometers. The spectrometer in Warsaw, Poland by Andrzejewski utilizes both a mini-orange magnet filter and a solenoid magnet to combine the advantages of the two methods [23]. The Australian National University has developed multiple spectrometers, each with unique approaches. One spectrometer incorporates the lens system with a superconducting solenoid [24] while another uses an electrostatic analyzer rather than a magnetic field to focus electrons [25]. The SPEDE spectrometer at CERN is unique in that it forgoes using fields completely to direct the electrons [26]. The original solenoid and orange spectrometer methods have continued to be used with some success. The SAGE spectrometer at the University of Jyväskylä [27] and the double orange spectrometer at the University of Cologne [28] are notable examples. These newer spectrometers have also been designed to allow coincidence measurements with gamma rays. Throughout these advancements, the mini-orange spectrometer has remained a popular method for conversion electron spectroscopy at various facilities [29–34]. In recent years, new mini-orange spectrometers have continued to be developed and used in experiments, including SPICE [35–37] at TRIUMF in Canada, the spectrometer at Sri Sathya Sai Institute of Higher Learning [38–40] in India, and SLICES [41,42] at the Legnaro National Laboratory in Italy.

Many of these spectrometers have used Si(Li) detectors as the primary detector choice due to silicon's low atomic number allowing for less backscattering [43]. In recent years, the use of silicon drift detectors (SDD) for conversion electron spectrometry has gained traction [44–49]. These detectors have the advantage of performing high-resolution measurements without liquid nitrogen cooling. While they are currently limited to low energy measurements, further development could lead to them becoming a viable detector option in the future.

The goal of this work was to build on the advances made for mini-orange spectrometers by using a combination of FreeCAD, COMSOL, and Geant4 simulations to improve on the efficiency of such a system.

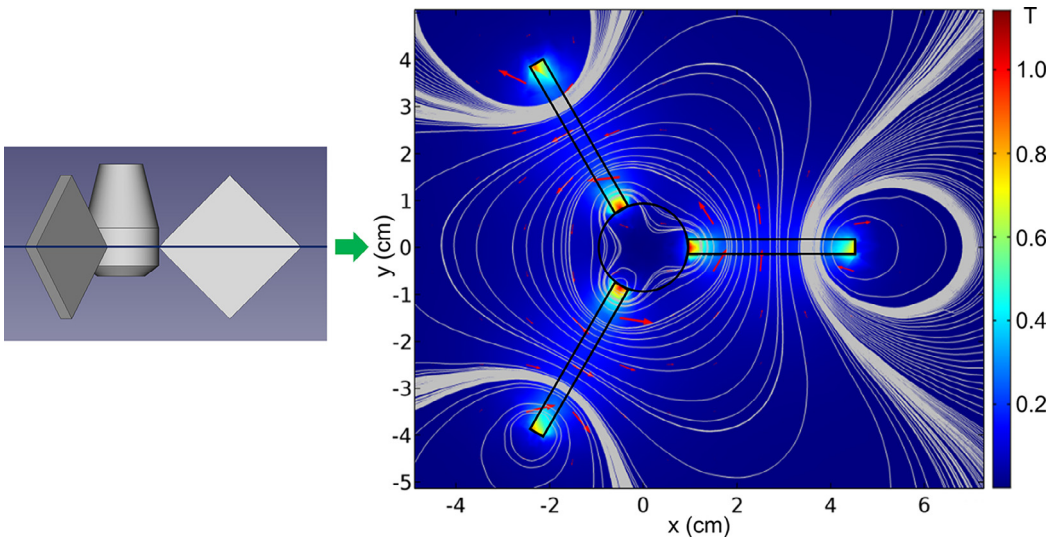

Fig. 3. 2-D snapshot of the magnetic field map simulated by COMSOL for one of the diamond shape magnet filters in ICEBall. This snapshot was taken at the middle plane of the filter indicated on the left figure by the blue line.

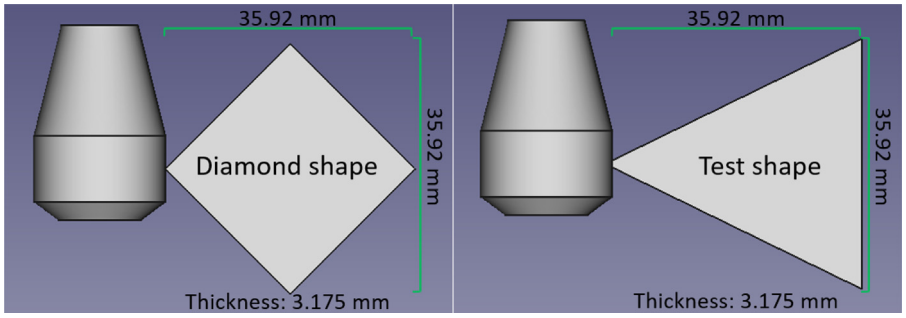

Fig. 4. Design constraints employed for the magnets based on the dimensions of the original diamond shape. The length and height of all magnet designs was restricted to a maximum of 35.92 mm due to the constraints of the spherical chamber. The thickness was also initially fixed to be uniform at 3.125 mm before that restriction was lifted.

This work started with the Internal Conversion Electron Ball Array (ICEBall) at the Nuclear Science Laboratory (NSL) at the University of Notre Dame. ICEBall contains closely packed Si(Li) detector arrangements in a small volume to allow close placement of Ge detectors to enhance the e-γ coincidence efficiency. The aim was to use simulations to improve on the efficiencies of the electron measurements.

2. ICEBall

ICEBall is a mini-orange spectrometer that was developed by Saladin and Metlay at the University of Pittsburgh in the 1990s [20]. It was designed to be used in coincidence measurements with gamma rays to improve identification and characterization of electromagnetic transitions depopulating excited states created in various nuclear reactions. In the early 2000s, it was moved to the Wright Nuclear Structure Laboratory at Yale University to be used with the YRAST Ball array [50]. During this time, ICEBall also saw use with the Spin Spectrometer at Oak Ridge National Laboratory [51] and Gammasphere at Argonne National Laboratory [52]. In 2010, it was moved to its current location, the NSL at the University of Notre Dame [53,54].

ICEBall consists of six Si(Li) detectors with six mini-orange magnet filters. A single pair consisting of a magnet filter and a Si(Li) detector is shown in Fig. 1. The Si(Li) detectors have an active area of 750 mm^2 and a thickness of 5 mm. The front is also covered with a thin aluminum Mylar foil. The magnet filter is positioned over the detector by a set of aluminum magnet holders. The filter consists of a central absorber made of tungsten and three diamond shaped $SmCo_5$ magnet wings, each with an area of 645.16 mm^2 (1 in^2) and thicknesses ranging from 3 to 4 mm. The tungsten absorber blocks the direct path from the source to the detector, blocking gamma rays, delta rays, and heavy particles. The field from the magnet wings bend the trajectory of electrons to increase the likelihood of them hitting the detector. The aluminum Mylar foil further helps by blocking low energy delta rays and secondary electrons. These six pairs are carefully positioned around a target mounted on a carbon graphite ladder that extends into the center of the chamber (Fig. 2). The distance from the target to each Si(Li) detector is 72 mm.

3. Magnet filter optimization

A major aspect of the increased electron detection efficiency is at the core of the transformation of ICEBall to fIREBall. It was speculated that significant improvement could be achieved by redesigning the magnet shapes that were used in the filters. The viability of using simulations to assess the performance of magnet filters was demonstrated in the development of SPICE (TRIUMF) [55] and SLICES (LNL) [41]. This work was inspired to follow suit and sought to similarly develop a set of simulations to fully test the viability and the resulting efficiency of implementing a wide variety of magnet shapes.

While Geant4 [56] is able to simulate the detection of electrons, it could not contribute to the calculation of magnetic fields resulting from the varying geometries of the magnet filters. Thus, it was used in combination with additional software to develop a simulation that could properly emulate a mini-orange spectrometer. FreeCAD [57] was used to construct the geometric designs of the magnet filters of varying shapes. The geometry was exported and loaded into COMSOL [58] to

Table 1
Conversion electron lines and their respective intensities that were considered for analysis. Energies and intensities were obtained from the evaluations done by NNDC based off of [59,60]. The 267 keV and 350 keV electron lines are a combination of several lines that were close to each other, with intensities used as weights. The total intensity was used for those two lines. The corresponding gamma energies are also listed. The radioactivity of each source was measured on March 4, 2021.

Source	Activity (Bq)	E_γ (keV)	E_{CE} (keV)	Intensity (%)
^{133}Ba	6720(68)	276.4	240.414	0.329(5)
		302.851	267.343	0.760(12)
		356.013	320.028	1.309
		356.013/383.849	350.043	0.421(2)
^{207}Bi	9508(40)	569.698	481.694	1.537(22)
		569.698	553.837	0.442(6)
		1063.656	975.651	7.08(17)
		1063.656	1047.795	1.84(5)

simulate the magnetic field generated from the magnet wings, which could then be exported as a 3-D field map (A 2-D snapshot is shown in Fig. 3). The geometry and the field maps were then imported into Geant4 to simulate the detection of electrons.

When generating the magnetic field map with COMSOL, the material of the magnet and its remanence (B_r) are needed as input parameters. While the current diamond shape magnets are made of $SmCo_5$, decisions were made to use grade N52 neodymium ($Nd_2Fe_{14}B$) for the new magnets. The remanences for $SmCo_5$ and grade N52 neodymium magnets are around 1.1 T and 1.46 T, respectively. These values were initially used when creating the field maps with COMSOL.

An example is illustrated in Fig. 4 with a few design constraints while designing the magnet shapes. These constraints were necessitated by the size of the ICEBall chamber and based off the dimensions of the original diamond shape magnets. Given that the maximum horizontal and vertical reach of the diamond shape was 35.92 mm ($\sqrt{2}$ in), it was decided that the length and height of the magnet designs at any point could not be greater than that same 35.92 mm in keeping with the external spherical chamber. The thicknesses of the magnets were also initially fixed to be uniform at 3.125 mm (1/8 in), based off the thickness of one of the original diamond shape magnets. However, that constraint was later removed to explore other potential shapes.

The simulation setup initially consisted of a single magnet filter and the active area of a Si(Li) detector inside a spherical chamber (top figure in Fig. 5). It was assumed that the efficiency was the same for all six detectors and the total efficiency could be approximated as six times the efficiency of one detector. The simulation was also designed to emulate the use of an electron source rather than a specific nuclear reaction. As such, parameters such as the beam direction and the angular distributions were not considered and electrons instead were generated at the center and fired at random directions over 4π. Each simulation run started with firing 1 000 000 electrons at 0.1 MeV. The absolute efficiency was obtained by tracking the number of electrons that hit the detector out of the total electrons fired. The energy of the electrons was then increased by 0.1 MeV and this process was repeated ten times until efficiencies were obtained over a range from 0.1 to 1.0 MeV. The simulation aimed to optimize the following parameters:

1. Cross-area shape of the magnet (max area of 1290.25 mm^2)
2. Number of wings (ranging from 3 to 6)
3. Thickness of the magnet (allowed to vary between 2 mm and 20 mm)

Approximately 500 different shapes were designed and tested using the simulation. Efficiency curves ranging from 0.1 to 1.0 MeV were obtained for every shape by plotting the efficiency against energy. Three shapes were then chosen and manufactured by Electron Energy Corporation to be experimentally tested. Each shape was intended for the following energy ranges (Fig. 6):

1. Shape 1: "Low energy" range (0.2–0.4 MeV)
2. Shape 2: "High energy" range (0.7–1.0 MeV)
3. Shape 3: "Overall" (0.2–1.0 MeV)

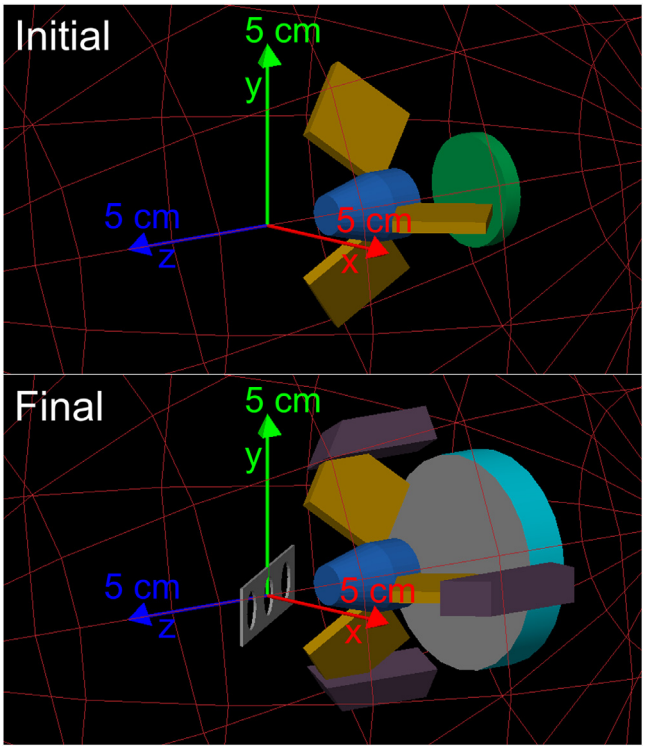

Fig. 5. Geant4 simulation setups were used to test the various magnet shapes. The top figure shows the first version that was used to test new shapes. The bottom figure shows the final version that was used to test the three chosen shapes after adding in the rest of the geometrical elements. Both versions consist of a single Si(Li) detector (active area in green, housing in cyan, foil in gray) and a magnet filter (magnets in gold, absorber in blue). The target ladder (gray) is also added in the final version as it could interfere with the trajectory of the electrons.

4. Comparison with simulation results

Experimental tests used a single magnet filter and Si(Li) detector to test the setup used in the simulation. In order to allow comparison with experiment and determine the improvement achieved by the three chosen magnet shapes, one of the current $SmCo_5$ diamond shape magnet filters was also included in this experiment. Three wing configurations were used for each shape. Two radioactive sources, ^{133}Ba and ^{207}Bi, were used for this experiment. Each source was mounted on the target ladder and positioned at the center of ICEBall. Data was collected in 90 min runs using a mesytec MDPP-16 module [61] with each source and each magnet shape. An example spectrum is shown in Fig. 7.

Table 1 lists the measured activities of the two radioactive sources used and the eight electron lines from the spectra that were considered for analysis. The activities were measured using a HPGe detector and three different sources with known activity and date of origin, ^{152}Eu, ^{60}Co, and a different ^{133}Ba. The three sources were used to obtain an efficiency calibration of the detector, which was then used to calculate the activity of the ^{133}Ba and ^{207}Bi sources used in the magnet filter tests. Information on the energies and intensities were obtained from [59] for ^{133}Ba and [60] for ^{207}Bi. For the 267 keV and 350 keV electron lines, there were several other electron lines listed that were close in energy. For those two cases, an average electron energy was calculated using the intensities as weights and the sum of the intensities was used as the overall intensity of that electron line.

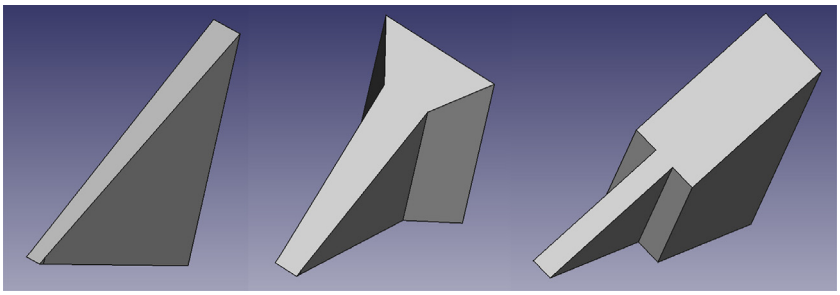

Fig. 6. From left to right: Shape 1, Shape 2, and Shape 3. From simulation results, shape 1 was intended for a range of 0.2–0.4 MeV, shape 2 was intended for 0.7–1.0 MeV, while shape 3 was intended for an energy range of 0.2–1.0 Mev. The efficiencies of each shape can be seen in Fig. 8.

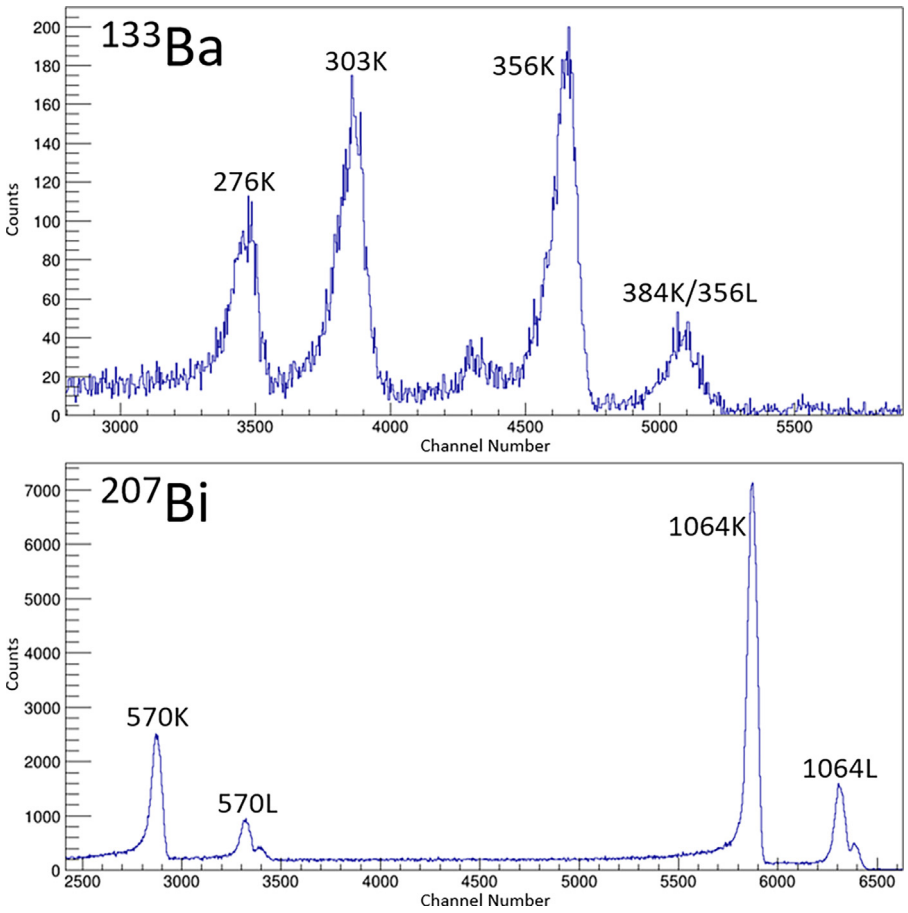

Fig. 7. Spectra of ^{133}Ba and ^{207}Bi obtained while testing one of the magnet filters. The exact energies and intensities of the eight peaks are shown in Table 1.

The following formula was used when calculating the absolute efficiency:

$$\text{Efficiency} = \frac{\text{Counts}}{\text{I} \times \text{A} \times \text{Time}} \quad (1)$$

where Counts is the total number of counts in the energy of interest, I is the intensity of the electron, A is the activity of the source, and Time is the run time. This was used to calculate both the efficiencies from the magnet filter tests and the activity of the ^{133}Ba and ^{207}Bi sources used in those tests. For all of these measurements, RadWare [62] was used to obtain the number of counts in every energy peak by applying a skewed Gaussian fit.

The simulations were further refined to better represent the spectrometer in ICEBall. Precise measurements of the alignment of the magnet wings with the absorber were made and accounted for in the CAD geometry. A gaussmeter was used to measure the magnetic field strength at the center point on the surface of each magnet wing. COMSOL was used to estimate an approximate remanence for each magnet from the measured magnet field strength. Table 2 lists the approximate remanence obtained for each magnet. While Shapes 2 and 3 had a remanence that was close to the initial value (1.46 T) used in COMSOL, Shape 1 was found to have a lower remanence. The diamond shape was found to have a higher remanence than the initial value (1.1 T). These remanences were re-inputted in COMSOL to generate a more accurate field map. In the Geant4 setup, every geometrical element that could potentially block an electron's path to the detector was included, such as the magnet filter holders, the end of target ladder located in the center of ICEBall, the complete housing of the SiLi detector, and the aluminum foil (bottom figure in Fig. 5). Simulations of the three chosen shapes were rerun at the energies from the two radioactive sources (Table 1) to obtain updated efficiency curves that could be plotted with the ones from experiment to allow a direct comparison.

Fig. 8 shows the comparison of the absolute efficiency curves obtained from the simulation and experiment for the three chosen shapes.

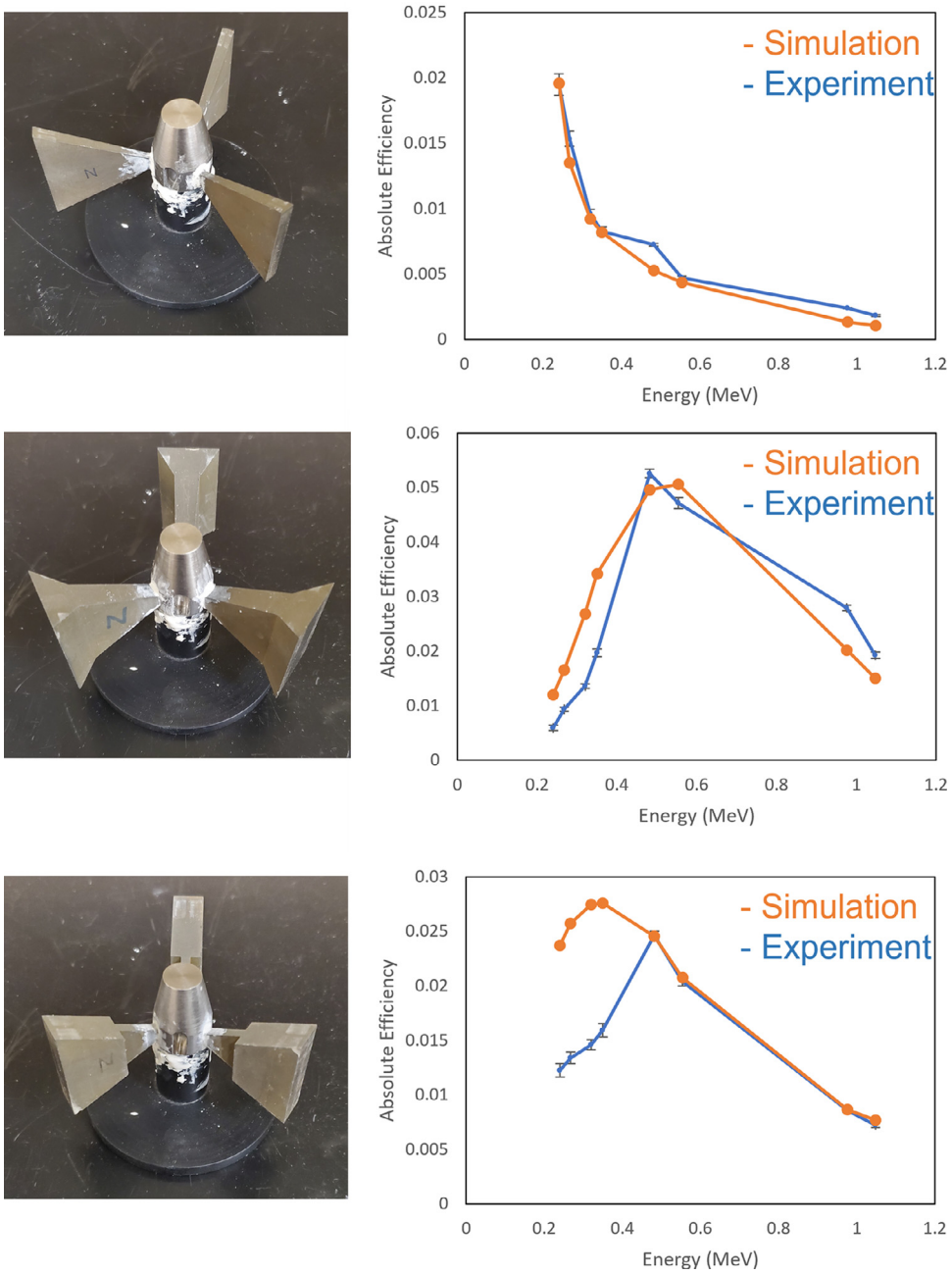

Fig. 8. Magnet filter configuration and the associated efficiency curves obtained from simulation and compared with experiment. From top to bottom, each row corresponds to Shape 1, Shape 2, and Shape 3.

Table 2
Remanence (B_r) of each magnet wing used in the experimental tests. While the remanence for Shapes 2 and 3 were close to the initial value (1.46 T) that was used in COMSOl, Shape 1 was found to have a lower remanence. The diamond shape was found to have a much higher remanence than the initial value (1.1 T).

Magnet shape	Remanence (T)
Diamond	1.48(3), 1.50(3), 1.51(3)
Shape 1	1.27(3), 1.25(3), 1.28(3)
Shape 2	1.47(3), 1.47(3), 1.51(3)
Shape 3	1.52(3), 1.54(3), 1.54(3)

Shape 1 showed the best agreement between its simulation and experiment efficiency curves out of the three shapes. The relative difference between the two efficiencies was the largest at 10% for the 481 keV electron line while it was within 7% for the other seven electron lines. Shape 2 showed reasonable agreement between its two efficiency curves. With the exception of the 320 and 350 keV electron lines from the ^{133}Ba source where the relative differences were nearly 30%, the differences for the remaining six electron lines was within 15%. Shape 3 was the most polarizing with the efficiencies from the ^{207}Bi source differing by less than 4% relatively, but those from the ^{133}Ba source differing by nearly 50%. It is possible that given the exotic geometries of Shape 2 and Shape 3, COMSOL is currently unable to accurately simulate the magnetic field generated. This would affect the efficiencies for the lower energy points more than the higher energy points as lower energy electrons are more susceptible to changes in the magnetic field.

Fig. 9 shows the comparison of the experimental efficiency curves for each shape along with the $SmCo_5$ diamond shape. Overall, Shape 2 outperformed all of the other shapes by achieving an absolute efficiency of at least 2% for five out of the eight energies (350 keV and above), reaching a peak absolute efficiency of 5.3% at 482 keV. This was nearly

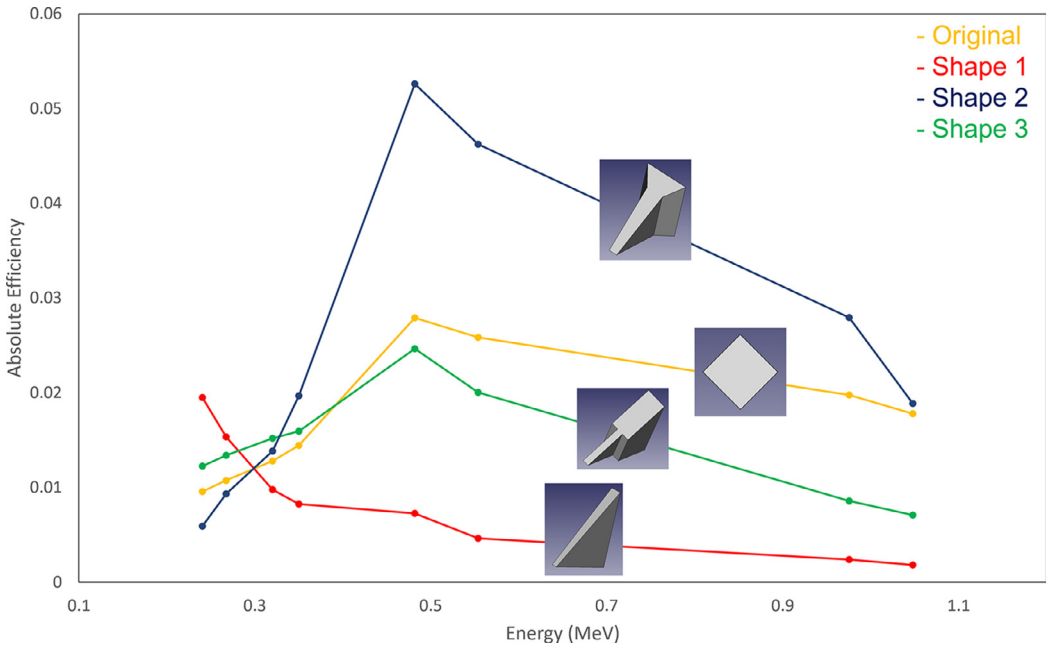

Fig. 9. Efficiency curves obtained from experiment for each shape, including the $SmCo_5$ diamond shape. The diamond shape has a higher efficiency than two of the chosen shapes at 482 keV and above, but not as high as the final chosen shape.

double the absolute efficiency of the diamond shape at that energy (2.8%). Shape 1 was the best performing shape for the low energies (267 keV and below), reaching a peak absolute efficiency of 2% at 240 keV, roughly doubling the absolute efficiency of the diamond shape at the same energy (1.0%). While Shape 3 was intended to be the one that was suited for all the energies, it was determined to be obsoleted by Shape 2 due to it only outperforming Shape 2 at low energies (320 keV and below) by less than 1% while being significantly outperformed for the other energies (350 keV and above). From these results, it was decided that Shape 2 would be used when assembling new magnet filters for fIREBall.

5. Conclusion

A combination of FreeCAD, COMSOL, and Geant4 simulations were used to determine the magnet shapes resulting in the greatest improvements in the efficiency of conversion electron detection. Three shapes, each intended for different criteria, were chosen to be tested in experiment and were found to be in good agreement with the results predicted by the simulations. A peak improvement of the absolute efficiency of ICEBall from 2.8% to 5.3% was achieved for the 482 keV K electron line, nearly a 100% improvement. Due to its performance, Shape 2 was chosen to be used in the new magnet filters. The new magnet filters along with the new detectors will transform ICEBall into the fIREBall array, which will be used to measure E0 transitions and conversion coefficients in the rare-earth region of nuclei to start. E0 measurements can be made more broadly to investigate pair production or branching ratios for $0^+ \rightarrow 0^+$ branching ratios in ^{10}C [63]. The latter is presently one of the largest errors in deducing the Cabibbo–Kobayashi–Maskawa (CKM) matrix unitarity which is one of the most sensitive tests of Physics beyond the standard model.

Declaration of competing interest

The authors declare that they have no known competing financial interests or personal relationships that could have appeared to influence the work reported in this paper.

Data availability

Data will be made available on request.

Acknowledgments

This research was funded under National Science Foundation, United States Grant PHY-2011890 and MRI Grant PHY-1919364. All of the work with COMSOL and Geant4 was completed through the Notre Dame Center for Research Computing. The authors also wish to thank Electron Energy Corporation for manufacturing the magnets.

References

[1] M. Scheck, P.A. Butler, L.P. Gaffney, N. Bree, R.J. Carrol, D. Cox, T. Grahn, P.T. Greenlees, K. Hauschild, A. Herzan, M. Huyse, U. Jakobsson, P. Jones, D.T. Joss, R. Julin, S. Juutinen, S. Ketelhut, R.-D. Herzberg, M. Kowalczyk, A.C. Larsen, M. Leino, A. Lopez-Martens, P. Nieminen, R.D. Page, J. Pakarinen, P. Papadakis, P. Peura, P. Rahkila, S. Rinta-Antila, P. Ruotsalainen, M. Sandzelius, J. Saren, C. Scholey, J. Sorri, J. Srebrny, P. Van Duppen, H.V. Watkins, J. Uusitalo, Combined in-beam electron and γ-ray spectroscopy of ^{184,186}Hg, Phys. Rev. C 83 (2011) 037303, http://dx.doi.org/10.1103/PhysRevC.83.037303.

[2] K. Heyde, J.L. Wood, Shape coexistence in atomic nuclei, Rev. Modern Phys. 83 (2011) 1467–1521, http://dx.doi.org/10.1103/RevModPhys.83.1467.

[3] W. Mampe, K. Schreckenbach, P. Jeuch, B. Maier, F. Braumandl, J. Larysz, T. von Egidy, The double focusing iron-core electron-spectrometer "BILL" for high resolution (n, e^-) measurements at the high flux reactor in Grenoble, Nucl. Instrum. Methods 154 (1978) 127–149, http://dx.doi.org/10.1016/0029-554X(78)90671-7.

[4] O. Klemperer, Electron beam spectroscopy, Rep. Progr. Phys. 28 (1965) 304, http://dx.doi.org/10.1088/0034-4885/28/1/304.

[5] E. Rutherford, H. Robinson, The analysis of the β rays from radium B and radium C, Lond. Edinb. Dublin Philos. Mag. J. Sci. 26 (1913) 717–729, http://dx.doi.org/10.1080/14786441308635016.

[6] R.A.R. Tricker, A helical method of focussing β-rays, Math. Proc. Camb. Phil. Soc. 22 (1924) 454–463, http://dx.doi.org/10.1017/S0305004100014365.

[7] O. Klemperer, The use of electron lenses for β-rays, Lond. Edinb. Dublin Philos. Mag. J. Sci. 20 (1935) 545–561, http://dx.doi.org/10.1080/14786443508561499.

[8] C.M. Witcher, An electron lens type of beta-ray spectrometer, Phys. Rev. 60 (1941) 32–42, http://dx.doi.org/10.1103/PhysRev.60.32.

[9] F.H. Schmidt, A uniform solenoidal magnetic field nuclear spectrometer, Rev. Sci. Instrum. 23 (1952) 361–366, http://dx.doi.org/10.1063/1.1746277.

[10] T. Lindblad, C. Lindén, An on-line multichannel electron spectrometer with high transmission, Nucl. Instrum. Methods 126 (1975) 397–406, http://dx.doi.org/10.1016/0029-554X(75)90703-X.

[11] C. Mallmann, Double beta coincidence spectrometer, Physica 18 (1952) 1139–1141, http://dx.doi.org/10.1016/S0031-8914(52)80188-0.

[12] M. Mladjenović, Recent developments of beta spectrometers, Nucl. Instrum. Methods 7 (1960) 11–21, http://dx.doi.org/10.1016/0029-554X(60)90064-1.

[13] K. Bisgård, Some data for a six gap beta ray spectrometer, Nucl. Instrum. Methods 22 (1963) 221–237, http://dx.doi.org/10.1016/0029-554X(63)90250-7.

[14] M. Metlay, Development of a Multiple-Element Conversion-Electron Spectrometer Array and Investigation of Transition Multipolarities in ^{130}Ce (Ph.D. thesis), University of Pittsburgh, 1992.

[15] R. Moore, S. Hayakawa, D. Rehfield, A high energy beta spectrometer using an intrinsic germanium crystal in a super-conducting solenoid, Nucl. Instrum. Methods 133 (1976) 457–464, http://dx.doi.org/10.1016/0029-554X(76)90430-4.

[16] Z. Árvay, T. Fényes, K. Füle, T. Kibédi, S. László, Z. Máté, G. Mórik, D. Novák, F. Tárkányi, An on-line Si(Li) electron spectrometer with superconducting magnet transporters, Nucl. Instrum. Methods 178 (1980) 85–93, http://dx.doi.org/10.1016/0029-554X(80)90860-5.

[17] M. Guttormsen, H. Hübel, A. Grumbkow, Y. Agarwal, J. Recht, K. Maier, H. Kluge, A. Maj, M. Menningen, N. Roy, A superconducting electron spectrometer, Nucl. Instrum. Methods Phys. Res. A 227 (1984) 489–498, http://dx.doi.org/10.1016/0168-9002(84)90206-7.

[18] V. Pelekhov, V. Moryakov, V. Martynenko, M. Sergeev, An economical helium cryostat for a superconducting solenoid of a conversion electron spectrometer, Nucl. Instrum. Methods Phys. Res. A 337 (1993) 101–105, http://dx.doi.org/10.1016/0168-9002(93)91141-9.

[19] J. van Klinken, K. Wisshak, Conversion electrons separated from high background, Nucl. Instrum. Methods 98 (1972) 1–8, http://dx.doi.org/10.1016/0029-554X(72)90416-8.

[20] M. Metlay, J. Saladin, I. Lee, O. Dietzsch, The ICEBall: a multiple element array for in-beam internal conversion electron spectroscopy, Nucl. Instrum. Methods Phys. Res. A 336 (1993) 162–170, http://dx.doi.org/10.1016/0168-9002(93)91092-2.

[21] J. van Klinken, S. Feenstra, K. Wisshak, H. Faust, Mini-orange spectrometers for in- and off-beam observation of conversion electrons, Nucl. Instrum. Methods 130 (1975) 427–441, http://dx.doi.org/10.1016/0029-554X(75)90040-3.

[22] J. van Klinken, S. Feenstra, G. Dumont, Wedge-shaped $SmCo_5$ magnets for mini-orange spectrometers, Nucl. Instrum. Methods 151 (1978) 433–438, http://dx.doi.org/10.1016/0029-554X(78)90152-0.

[23] J. Andrzejewski, A. Król, J. Perkowski, K. Sobczak, R. Wojtkiewicz, M. Kisieliński, M. Kowalczyk, J. Kownacki, A. Korman, Electron spectrometer for "in-beam" spectroscopy, Nucl. Instrum. Methods Phys. Res. A 585 (2008) 155–164, http://dx.doi.org/10.1016/j.nima.2007.11.011.

[24] T. Kibédi, G. Dracoulis, A. Byrne, Lens-mode operation of a superconducting electron spectrometer in (HI, xn) reactions, Nucl. Instrum. Methods Phys. Res. A 294 (1990) 523–533, http://dx.doi.org/10.1016/0168-9002(90)90294-G.

[25] B.P.E. Tee, A.E. Stuchbery, M. Vos, J.T.H. Dowie, B.Q. Lee, M. Alotiby, I. Greguric, T. Kibédi, High-resolution conversion electron spectroscopy of the ^{125}I electron-capture decay, Phys. Rev. C 100 (2019) 034313, http://dx.doi.org/10.1103/PhysRevC.100.034313.

[26] P. Papadakis, D.M. Cox, G.G. O'Neill, M.J.G. Borge, P.A. Butler, L.P. Gaffney, P.T. Greenlees, R.D. Herzberg, A. Illana, D.T. Joss, J. Konki, T. Kröll, J. Ojala, R.D. Page, P. Rahkila, K. Ranttila, J. Thornhill, J. Tuunanen, P. Van Duppen, N. Warr, J. Pakarinen, The SPEDE spectrometer, Eur. Phys. J. A 54 (2018) 42, http://dx.doi.org/10.1140/epja/i2018-12474-9.

[27] J. Pakarinen, P. Papadakis, J. Sorri, R.D. Herzberg, P.T. Greenlees, P.A. Butler, P.J. Coleman-Smith, D.M. Cox, J.R. Cresswell, P. Jones, R. Julin, J. Konki, I.H. Lazarus, S.C. Letts, A. Mistry, R.D. Page, E. Parr, V.F.E. Pucknell, P. Rahkila, J. Sampson, M. Sandzelius, D.A. Seddon, J. Simpson, J. Thornhill, D. Wells, The SAGE spectrometer, Eur. Phys. J. A 50 (2014) 53, http://dx.doi.org/10.1140/epja/i2014-14053-6.

[28] J.-M. Régis, T. Materna, G. Pascovici, S. Christen, A. Dewald, C. Fransen, J. Jolie, P. Petkov, K.O. Zell, Improvement of the intrinsic time resolving power of the cologne iron-free orange type electron spectrometers, Rev. Sci. Instrum. 81 (2010) 113505, http://dx.doi.org/10.1063/1.3499259.

[29] E. Ditzel, J. Hoogduin, H. Backe, F. de Boer, H. Bokemeyer, M. Debowski, J. van Klinken, P. Salabura, H. Wollersheim, H. Xie, Doppler-corrected spectroscopy of conversion electrons with mini-oranges after heavy-ion collisions, Nucl. Instrum. Methods Phys. Res. A 376 (1996) 428–433, http://dx.doi.org/10.1016/0168-9002(96)00260-4.

[30] M. Metlay, L. Riley, P. Cottle, J. Jewell, K. Kemper, Zero degree detector for conversion-electrons from a heavy-ion-induced reaction, Nucl. Instrum. Methods Phys. Res. A 385 (1997) 112–115, http://dx.doi.org/10.1016/S0168-9002(96)00792-9.

[31] B. Aengenvoort, W. Korten, H. Hübel, S. Chmel, A. Görgen, U. van Severen, W. Pohler, R. Zinken, T. Härtlein, C. Ender, F. Köck, P. Reiter, D. Schwalm, F. Schindler, J. Gerl, R. Schubart, F. Azaiez, S. Bouneau, J. Duprat, I. Deloncle, Conversion-electron gamma-ray coincidence spectroscopy of superdeformed ^{135}Nd, Eur. Phys. J. A 1 (1998) 359–364, http://dx.doi.org/10.1007/s100500050070.

[32] D. Gassmann, P. Thirolf, E. Mergel, D. Habs, M. Chromik, J. Domscheit, A. Görgen, K. Hauschild, H. Hübel, M. Hunyadi, A. Krasznahorkay, A. Lopez-Martens, S. Neumann, A. Neußer, D. Pansegrau, P. Reiter, H. Scheit, G. Schönwaßer, D. Schwalm, Conversion electron spectroscopy in the superdeformed minimum of ^{240}Pu, Phys. Lett. B 497 (2001) 181–189, http://dx.doi.org/10.1016/S0370-2693(00)01353-8.

[33] D.R. Rao, K.V. Sai, M. Sainath, R. Gowrishankar, K. Venkataramaniah, Electron-gamma spectroscopic measurements in ^{131}Cs, Appl. Radiat. Isot. 66 (2008) 377–388, http://dx.doi.org/10.1016/j.apradiso.2007.09.016.

[34] W. Schwerdtfeger, P.G. Thirolf, K. Wimmer, D. Habs, H. Mach, T.R. Rodriguez, V. Bildstein, J.L. Egido, L.M. Fraile, R. Gernhäuser, R. Hertenberger, K. Heyde, P. Hoff, H. Hübel, U. Köster, T. Kröll, R. Krücken, R. Lutter, T. Morgan, P. Ring, Shape coexistence near neutron number n = 20: First identification of the E0 decay from the deformed first excited $J^\pi = 0^+$ state in 30Mg, Phys. Rev. Lett. 103 (2009) 012501, http://dx.doi.org/10.1103/PhysRevLett.103.012501.

[35] A. Garnsworthy, M. Moukaddam, C. Bolton, S. Ketelhut, L. Evitts, C. Andreoiu, M. Constable, G. Hackman, R. Henderson, C. Svensson, The SPICE Detector at ISAC, in: C. Simenel, M. Evers, T. Kibédi, D.H. Luong, M. Reed, M. Srncik, A. Wallner (Eds.), EPJ Web Conf. 63 (2013) 01010, http://dx.doi.org/10.1051/epjconf/20136301010.

[36] M. Moukaddam, J. Smallcombe, L.J. Evitts, A.B. Garnsworthy, C. Andreoiu, G.C. Ball, J. Berean-Dutcher, D. Bishop, C. Bolton, R. Caballero-Folch, M. Constable, D.S. Cross, T.E. Drake, R. Dunlop, P.E. Garrett, S. Georges, G. Hackman, S. Hallam, J. Henderson, R. Henderson, R. Krücken, L. Kurchaninov, A. Kurkjian, B. Olaizola, E. O'Sullivan, P. Lu, J. Park, E.E. Peters, J.L. Pore, E.T. Rand, P. Ruotsalainen, J.K. Smith, D. Southall, M. Spencer, C.E. Svensson, M. Wiens, M. Williams, S.W. Yates, T. Zidar, In-beam internal conversion electron spectroscopy with the SPICE detector, Nucl. Instrum. Methods Phys. Res. A 905 (2018) 180–187, http://dx.doi.org/10.1016/j.nima.2018.07.064.

[37] J. Smallcombe, A.B. Garnsworthy, W. Korten, P. Singh, F.A. Ali, C. Andreoiu, S. Ansari, G.C. Ball, C.J. Barton, S.S. Bhattacharjee, M. Bowry, R. Caballero-Folch, A. Chester, S.A. Gillespie, G.F. Grinyer, G. Hackman, C. Jones, B. Melon, M. Moukaddam, A. Nannini, P. Ruotsalainen, K. Starosta, C.E. Svensson, R. Wadsworth, J. Williams, Improved measurement of the $0_2^+ \rightarrow 0_1^+$ E0 transition strength for ^{72}Se using the SPICE spectrometer, Phys. Rev. C 106 (2022) http://dx.doi.org/10.1103/PhysRevC.106.014312.

[38] K. Venkataramaniah, M. Sainath, K. Sai, D. Rao, D. Seetharaman, Design and development of a mini-orange magnetic spectrometer with multichannel facility for conversion electron spectroscopy, J. Nucl. Phys. Mater. Sci. Radiat. Appl. 8 (2020) 25–31, http://dx.doi.org/10.15415/jnp.2020.81004.

[39] K.M. Rao, K.V. Sai, E. Rajasekhar, D. Seetharaman, D.R. Rao, K. Venkataramaniah, New measurements of internal conversion coefficients in ^{111}Cd, Phys. Atom. Nucl. 84 (2021) 817–825, http://dx.doi.org/10.1134/S1063778821130287.

[40] S. Deepa, K.V. Sai, D.R. Rao, K.M. Rao, K. Venkataramaniah, EC-decay of ^{133}Ba revisited by electron-gamma spectroscopy, J. Radioanal. Nucl. Chem. 328 (2021) 1001–1010, http://dx.doi.org/10.1007/s10967-021-07731-x.

[41] N. Marchini, A. Nannini, M. Ottanelli, A. Saltarelli, M. Rocchini, G. Benzoni, E. Gamba, A. Goasduff, A. Gottardo, T. Krings, M. Perri, SLICES: Spes low-energy internal conversion electron spectrometer, Nucl. Instrum. Methods Phys. Res. A 1020 (2021) 165860, http://dx.doi.org/10.1016/j.nima.2021.165860.

[42] N. Marchini, A. Nannini, M. Ottanelli, A. Saltarelli, G. Benzoni, E.R. Gamba, A. Goasduff, A. Gottardo, J. Ha, T. Krings, M. Perri, M. Polettini, M. Rocchini, P. Sona, Electric monopole transitions and structure of low-spin states in ^{106}Pd, Phys. Rev. C 105 (2022) 054304, http://dx.doi.org/10.1103/PhysRevC.105.054304.

[43] G. Knoll, Radiation Detection and Measurement, fourth ed., Wiley, 2010.

[44] K. Peräjärvi, J. Turunen, S. Ihantola, V. Kämäräinen, S. Pommé, R. Pöllänen, T. Siiskonen, H. Sipilä, H. Toivonen, Feasibility of conversion electron spectrometry using a peltier-cooled silicon drift detector, J. Radioanal. Nucl. Chem. 299 (2014) 229–234, http://dx.doi.org/10.1007/s10967-013-2788-0.

[45] S. Pommé, J. Paepen, K. Peräjärvi, J. Turunen, R. Pöllänen, Conversion electron spectrometry of pu isotopes with a silicon drift detector, Appl. Radiat. Isot. 109 (2016) 183–188, http://dx.doi.org/10.1016/j.apradiso.2015.11.052.

[46] S. Pommé, M. Marouli, J. Paepen, N. Marković, R. Pöllänen, Deconvolution of ^{238,239,240}Pu conversion electron spectra measured with a silicon drift detector, Appl. Radiat. Isot. 134 (2018) 233–239, http://dx.doi.org/10.1016/j.apradiso.2017.08.033.

[47] H. Zhang, R. Wu, W. Wan, T. Feng, W. Lei, Y. Wang, B. Long, J. Yin, J. Zhan, J. Zhou, Application of a silicon drift detector to measuring internal conversion electrons and analysis of their spectra, Nucl. Instrum. Methods Phys. Res. A 950 (2020) 162941, http://dx.doi.org/10.1016/j.nima.2019.162941.

[48] M. Gugiatti, M. Biassoni, M. Carminati, O. Cremonesi, C. Fiorini, P. King, P. Lechner, S. Mertens, L. Pagnanini, M. Pavan, S. Pozzi, Characterisation of a silicon drift detector for high-resolution electron spectroscopy, Nucl. Instrum. Methods Phys. Res. A 979 (2020) 164474, http://dx.doi.org/10.1016/j.nima.2020.164474.

[49] S. Mertens, T. Brunst, M. Korzeczek, M. Lebert, D. Siegmann, A. Alborini, K. Altenmüller, M. Biassoni, L. Bombelli, M. Carminati, M. Descher, D. Fink, C. Fiorini, C. Forstner, M. Gugiatti, T. Houdy, A. Huber, P. King, O. Lebeda, P. Lechner, V.S. Pantuev, D.S. Parno, M. Pavan, S. Pozzi, D.C. Radford, M. Slezák, M. Steidl, P. Trigilio, K. Urban, D. Vénos, J. Wolf, S. Wüstling, Y.-R. Yen, Characterization of silicon drift detectors with electrons for the TRISTAN project, J. Phys. G: Nucl. Part. Phys. 48 (2021) 015008, http://dx.doi.org/10.1088/1361-6471/abc2dc.

[50] C.W. Beausang, New instruments and devices at the wright nuclear structure laboratory, AIP Conf. Proc. 680 (2003) 1022–1025, http://dx.doi.org/10.1063/1.1619882.

[51] J.X. Saladin, M.P. Metlay, D.F. Winchell, M.S. Kaplan, I.Y. Lee, C. Baktash, M.L. Halbert, N.R. Johnson, O. Dietzsch, Evidence for continuum E0 transitions following the decay of high spin states in 130Ce, Phys. Rev. C 53 (1996) 652–659, http://dx.doi.org/10.1103/PhysRevC.53.652.

[52] G. Gürdal, C.W. Beausang, D.S. Brenner, H. Ai, R.F. Casten, B. Crider, A. Heinz, E. Williams, D.J. Hartley, M.P. Carpenter, A.A. Hecht, R.V.F. Janssens, T. Lauritsen, C.J. Lister, R. Raabe, D. Seweryniak, S. Zhu, J.X. Saladin, Measurement of conversion coefficients in normal and triaxial strongly deformed bands in ^{167}Lu, Phys. Rev. C 77 (2008) 024314, http://dx.doi.org/10.1103/PhysRevC.77.024314.

[53] A. Battaglia, W. Tan, R. Avetisyan, C. Casarella, A. Gyurijinyan, K.V. Manukyan, S.T. Marley, A. Nystrom, N. Paul, K. Siegl, K. Smith, M.K. Smith, S.Y. Strauss, A. Aprahamian, Measurements of conversion electrons in the s-process branching point nucleus ^{176}Lu, Eur. Phys. J. A 52 (2016) 126, http://dx.doi.org/10.1140/epja/i2016-16126-x.

[54] S. Strauss, Conversion Electrons in ^{154,156}Gd (Ph.D. thesis), 2020.

[55] S. Ketelhut, L. Evitts, A. Garnsworthy, C. Bolton, G. Ball, R. Churchman, R. Dunlop, G. Hackman, R. Henderson, M. Moukaddam, E. Rand, C. Svensson, J. Witmer, Simulated performance of the in-beam conversion-electron spectrometer, SPICE, Nucl. Instrum. Methods Phys. Res. A 753 (2014) 154–163, http://dx.doi.org/10.1016/j.nima.2014.03.001.

[56] S. Agostinelli, J. Allison, K. Amako, J. Apostolakis, H. Araujo, P. Arce, M. Asai, D. Axen, S. Banerjee, G. Barrand, F. Behner, L. Bellagamba, J. Boudreau, L. Broglia, A. Brunengo, H. Burkhardt, S. Chauvie, J. Chuma, R. Chytracek, G. Cooperman, G. Cosmo, P. Degtyarenko, A. Dell'Acqua, G. Depaola, D. Dietrich, R. Enami, A. Feliciello, C. Ferguson, H. Fesefeldt, G. Folger, F. Foppiano, A. Forti, S. Garelli, S. Giani, R. Giannitrapani, D. Gibin, J.G. Cadenas, I. González, G.G. Abril, G. Greeniaus, W. Greiner, V. Grichine, A. Grossheim, S. Guatelli, P. Gumplinger, R. Hamatsu, K. Hashimoto, H. Hasui, A. Heikkinen, A. Howard, V. Ivanchenko, A. Johnson, F. Jones, J. Kallenbach, N. Kanaya, M. Kawabata, Y. Kawabata, M. Kawaguti, S. Kelner, P. Kent, A. Kimura, T. Kodama, R. Kokoulin, M. Kossov, H. Kurashige, E. Lamanna, T. Lampén, V. Lara, V. Lefebure, F. Lei, M. Liendl, W. Lockman, F. Longo, S. Magni, M. Maire, E. Medernach, K. Minamimoto, P.M. de Freitas, Y. Morita, K. Murakami, M. Nagamatu, R. Nartallo, P. Nieminen, T. Nishimura, K. Ohtsubo, M. Okamura, S. O'Neale, Y. Oohata, K. Paech, J. Perl, A. Pfeiffer, M. Pia, F. Ranjard, A. Rybin, S. Sadilov, E.D. Salvo, G. Santin, T. Sasaki, N. Savvas, Y. Sawada, S. Scherer, S. Sei, V. Sirotenko, D. Smith, N. Starkov, H. Stoecker, J. Sulkimo, M. Takahata, S. Tanaka, E. Tcherniaev, E.S. Tehrani, M. Tropeano, P. Truscott, H. Uno, L. Urban, P. Urban, M. Verderi, A. Walkden, W. Wander, H. Weber, J. Wellisch, T. Wenaus, D. Williams, D. Wright, T. Yamada, H. Yoshida, D. Zschiesche, Geant4—a simulation toolkit, Nucl. Instrum. Methods Phys. Res. A 506 (2003) 250–303, http://dx.doi.org/10.1016/S0168-9002(03)01368-8.

[57] FreeCAD. URL https://www.freecadweb.org/.

[58] COMSOL multiphysics. URL https://www.comsol.com/.

[59] Y. Khazov, A. Rodionov, F. Kondev, Nuclear data sheets for A = 133, Nucl. Data Sheets 112 (2011) 855–1113, http://dx.doi.org/10.1016/j.nds.2011.03.001.

[60] F. Kondev, S. Lalkovski, Nuclear data sheets for A = 207, Nucl. Data Sheets 112 (2011) 707–853, http://dx.doi.org/10.1016/j.nds.2011.02.002.

[61] A. Ruben, P.C. Bender, P. Chowdhury, P.L. Kerr, F. Lüke, G. Montermann, A.M. Rogers, R. Schneider, A new, versatile, high-performance digital pulse processor with application to neutron/Gamma-ray pulse-shape discrimination in scintillator detectors, 2018, URL https://www.mesytec.com/products/appnotes/MDPP16_SORMA_2018.pdf.

[62] D. Radford, RadWare. URL https://radware.phy.ornl.gov/main.html.

[63] J.C. Hardy, I.S. Towner, Superallowed $0^+ \rightarrow 0^+$ nuclear β decays: A new survey with precision tests of the conserved vector current hypothesis and the standard model, Phys. Rev. C 79 (2009) 055502, http://dx.doi.org/10.1103/PhysRevC.79.055502.